Taylor & Francis
Taylor & Francis Group

RESEARCH ARTICLE

OPEN ACCESS | Check for updates

(-)-Epigallocatechin-3-gallate encapsulated realgar nanoparticles exhibit enhanced anticancer therapeutic efficacy against acute promyelocytic leukemia

Wei Fang[a], Zhao Liang Peng[b], Ya Ji Dai[c], Dian Lei Wang[a,d], Peng Huang[a] and He Ping Huang[a]

[a]The College of Pharmacy, Anhui University of Chinese Medicine, Hefei, Anhui, China; [b]Chinese Academy of Sciences Shanghai Institute of Materia Medica, ShangHai, China; [c]Anhui Second People's Hospital, HeFei, Anhui, China; [d]Anhui Province Key Laboratory of Chinese Medicinal Formula, Hefei, Anhui, China

ABSTRACT

Realgar and (-)-Epigallocatechin-3-gallate (EGCG) are natural medicines that inhibit cancer cell growth, resulting in inhibition of formation and development of tumors. The anticancer effects of realgar and EGCG were greatly improved following formulation as nanoparticles. EGCG has received increased attention as a drug carrier. The aim of this study was to prepare a new nanomedicine, (EGCG-RNPs), in which encapsulated nano-realgar. EGCG-RNPs were prepared by coprecipitation and characterized by transmission electron microscopy (TEM), differential scanning calorimetry (DSC), particle size and zeta potential, X-ray diffraction, Fourier transform infrared spectroscopy (FTIR) and in vitro release. Furthermore, we evaluated the antiproliferative effects of EGCG-RNPs on HL-60 cells in vitro, antitumor effect by intratumoral injection of EGCG-RNPs into solid tumors derived from APL HL-60 cells in vivo. Possible mechanisms were evaluated using uptake and efflux experiments in HL-60 cells. The results showed that the average particle size and zeta potentials of EGCG-RNPs was 200.3 ± 1.23 nm and -46.8 ± 1.31 mV. Controlled release of EGCG-RNPs was sustained and continued up to 72 h in vitro. Compared with nano-realgar and EGCG + RNPs (EGCG and nano-realgar physical mixing), EGCG-RNPs significantly inhibited growth of HL-60 cells. In a solid tumor model, EGCG-RNPs decreased tumor volumes, with an inhibitory rate of 60.18% at a dose of $70\, mg \cdot kg^{-1}$. The mechanisms of antitumor improvement may correlate with the increased uptake of realgar and prolonged the retention time of realgar in HL-60 cells due to EGCG as a carrier. EGCG-RNPs could enhance anticancer therapeutic efficacy for acute promyelocytic leukemia.

Introduction

Acute promyelocytic leukemia (APL), a subtype of acute myeloid leukemia (AML), characterized by the balanced translocation t (15;17)(q22;q12) resulting in the fusion transcript PML-RARA, is a common hematopoietic disease with severe and complicated clinical considerations (Mauro, 2005). Chemotherapy is the main treatment for leukemia. However, there are no good options for reversing multidrug resistance, prolonging or preventing leukemia recurrence, or preventing leukemia-related complications (Tallman et al., 2002). Recently, EGCG and arsenic preparations have shown promise for treatment of acute promyelocytic leukemia (Mcculloch et al., 2017; Moradzadeh et al., 2017).

Realgar (Xiong Huang), a traditional Chinese medicine is composed primarily of tetraarsenic tetra-sulfide (As_4S_4). Mainly include different forms of mineral arsenicals (orpiment-As_2S_3, realgar-As_4S_4, and arsenolite-arsenic trioxide, As_2O_3) are used (Jie et al., 2011). Realgar is insoluble in water and most organic solvents, resulting in poor bioavailability

clinical application (Tanaka et al., 2000; Shen et al., 2001). Recent studies have shown that realgar exerts antitumor effects. Realgar enhances leukemia and solid tumor sensitivity to chemotherapeutic drugs by regulating key apoptosis genes, as evidenced by DNA fragmentation, depletion of the mitochondrial membrane potential, cleavage of caspases and ant apoptosis proteins, inhibition of tumor angiogenesis, and induction of tumor cell death (Philipp et al., 2015). Enhanced solubility or nanoparticulate preparations may improve the therapeutic potential of realgar (Baláž et al., 2009).

(-)-Epigallocatechin-gallate (EGCG), a phenolic compound, is the most abundant and bioactive catechin among tea polyphenols (Higdon and Balz, 2003). EGCG can arrest cancer cell growth and promote maturation and differentiation of cancer cells (Kazushige, 2005; Chih-Yeu et al., 2015; Dongxu et al., 2015). Recently, EGCG has been used as a drug carrier or as a dispersant to enhances the effects of other drugs drew great attention (Hajipour et al., 2018). Studies have demonstrated that EGCG combined with metal ions such as

---

CONTACT Dianlei Wang ✉ dlwang@ahtcm.edu.cn; Peng Huang ✉ great7701@126.com The College of Pharmacy, Anhui University of Chinese Medicine, Qianjiang road 001, Hefei, Anhui, 230012, China

Supplemental data for this article can be accessed here.

Fe^{3+} or Mn^{2+} to form complexes by gallate ring may enhance biological activity and reduce metal toxicity (Ryan and Hynes, 2007). One example is 198AuNP-EGCG, which is a nanotherapeutic formulation effective for treatment of prostate solid tumors (Hsieh et al., 2012; Ravi et al., 2012). EGCG can also act as a dispersant in EGCG-dispersed selenium nanoparticles (Shanshan et al., 2013). To increase the antimicrobial activity and stability of EGCG, an EGCG-Cu(II) complex was formed by chelating copper ions with EGCG (Acevedo et al., 2018). These complexes were then electronspun into polyvinyl alcohol (PVA) nanofibers(EGCG-CuII/PVA) (Sun et al., 2011). EGCG and its derivatives are promising candidates for development of effective and nontoxic medicines with strong free-radical scavenging and antioxidant abilities (Bing et al., 2013). EGCG enhances differentiation of acute promyelocytic leukemia cells via inhibition of PML-RAR-alpha/PML proteins, HDAC1, PTEN (Farabegoli et al., 2010; Yao et al., 2017).

We evaluated the antiproliferative effects of nano-realgar encapsulated in EGCG (EGCG-RNPs) with solid tumors. In this study, developed a novel method for preparation of EGCG-RNPs and evaluated their inhibitory effects on APL HL-60 cells. Uptake and efflux in HL-60 cells was evaluated. Furthermore, we established a subcutaneous solid tumor model in NOD/SCID nude mice and evaluated the inhibitory effects of EGCG-RNPs injection directly into the tumor site, as determined by tumor volume and weight (Scheme 1). This innovative nanotechnological approach may serve as a basis for designing target specific antineoplastic agents. The oncological implications for treating APL HL-60 cell solid tumors and other solid tumors will be discussed.

Materials and methods

Reagents

Epigallocatechin gallate (EGCG) (purity 99.99%) (Sigma, USA); Realgar (As_4S_4, Anhui Bozhou Chinese herbal medicine market); Chromatography grade methanol (Shanghai Star Company, 20170802); Arsenic standard stock solution (Shanghai Institute of Metrology, 0511, $1\,mg \cdot mL^{-1}$); Nitric acid (Sinopharm Group, GR, 20170117); Hydrochloric acid (Sinopharm Group, GR, 20170117); Germanium ($1\,mg \cdot mL^{-1}$) (Shanghai Institute of Metrology, 0632); Phosphate-buffered saline (PBS, prepared in our laboratory); all other reagents were of analytical grade.

Cell

HL-60 cells (China Center for Type Culture Collection);Fetal bovine serum (FBS) (GIBCO, No. 16000-044); Methyl sulfoxide (US Sigma Corporation, 20170210); Dimethyl sulfoxide (US Sigma Corporation, 20170610); Thiazolyl Blue Tetrazolium Bromide (MTT, American Sigma company, MKB06849V); Iscove's Modified Dulbecco's Medium (IMDM, US HyClone, AB212851); Phosphate-buffered saline (PBS, prepared in our laboratory); Ethanol (Guangdong Xinyuan Chemical, 20160801).

Animal

NOD/SCID mice were produced by hybridization of Severe Combined Immunodeficiency (SCID) mice and Nonobese Diabetes mellitus (NOD/lt) mice. This provided favorable conditions for establishment of a solid tumor model based on HL-60 cells. All protocols and animal care were in accordance with the Guidelines for the Use of Laboratory Animals (National Research Council) and authorized by the Animal Care and Use Committee of Anhui University of Chinese Medicine. Forty-five NOD/SCID mice (6 weeks old) were purchased from the Nanjing University-Nanjing Institute of Biomedicine (Nanjing, China). All NOD/SCID mice were acclimated in an animal breeding room under specific pathogen-free (SPF) conditions (Laboratory License No. SYXK (Su) 2016-0014). Animal Certificate No.: 201800222. Laboratory animal production license No.: SCXK (Su) 2017-0001. The special pellet feed was sterilized by cobalt 60 radiation (Jiangning (Nanjing) Qinglongshan feed).

Preparation of EGCG-RNPs

Chemical precipitation was used to purify and prepare the nano-realgar, resulting in uniform particle size distribution. EGCG-RNPs were prepared by chemical coprecipitation method. In brief, mixed solution of the nano-realgar purified solution(preparation methods refer to previous studies) (Wang et al., 2008), deionized water and EGCG was stirred, and diluted HCl was slowly injected to facilitate dissolution. The mixed solution was a light blue milky color/consistency. The solution was lyophilized using a vacuum freeze dryer (Marin Christ, Germany, model: Alpha 1-2LD).

Particle size and zeta potential

Determination of average particle size, polydispersity index (PDI), and zeta potential of EGCG-RNPs ($1\,mg \cdot mL^{-1}$) was performed using a Malvern particle size analyzer (Zetasizer 3000HS; Malvern Instruments, UK). Each experiment was performed in triplicate ($n = 3$) at $25\,°C$.

Transmission electron microscopy

Physical appearance and nanoparticle size distribution were evaluated using a transmission electron microscope (TEM, SU8200, Hitachi TEM system; Hitachi High-Technologies). Solutions of nano-realgar and EGCG-RNPs were diluted to optimal concentrations with absolute alcohol and placed on a copper grid prior to analysis.

Differential scanning calorimetry

Differential scanning calorimetry (DSC) was used to perform thermal analysis (Nexus, Germany DSC200F3). Samples (EGCG-RNPs, nano-realgar, EGCG + RNPs and EGCG, all solid powders) were accurately weighed, placed in aluminum pans, and sealed. DSC thermograms were obtained across the range of $25–300\,°C$ in a nitrogen atmosphere with a

temperature gradient of $10\,^{\circ}C \cdot min^{-1}$, to determine the glass transition temperature.

X-ray diffraction analysis

EGCG-RNPs were lyophilized with glucose as a cryoprotectant using a vacuum freeze dryer (Marin Christ, Germany, model: Alpha 1-2LD) prior to scanning. X-ray diffraction analysis (XRD) of the samples (EGCG-RNPs, traditional realgar, nano-realgar, EGCG + RNPs and EGCG, solid powder) was performed using an X-ray diffractometer (Bruker, Germany) equipped with a Cu Kα radiation source.

Fourier transform infrared spectroscopy

For further confirm the possible way of complexes formation between EGCG and nano-realgar, FTIR (Thermo Nicolet 6700 Thermo Fisher Scientific, USA) spectral analysis of EGCG-RNPs, Nano-realgar, EGCG, and EGCG + RNPs was performed.

Controlled release and drug loading

In vitro release of nano-realgar from EGCG-RNPs were determined using a dialysis device with a 100 kDa molecular weight cutoff in 150 mL of PBS solution (pH 7.4) at 37 °C to mimic physiological environments. Nano-realgar release was investigated comparing release of realgar from EGCG-RNPs with that of free nano-realgar (Zhou et al., 2013). Control bags were prepared and tested in parallel. Each control bag contained 0.1 mg of nano-realgar. At predetermined time intervals, the release medium was withdrawn for analysis. After sample treatment, the cumulative release rate (M_n) and cumulative release percentage (Q_n) were fitted according to Equation (1) and Equation (2).

$$M_n = C_n V_0 + \sum_{i}^{n} C_i V_i \tag{1}$$

$$Q_n = M_n / V_0 \times 100\% \tag{2}$$

Where M_n is cumulative release at each time point. C_n is the measured drug concentration at the nth time point, V_0 is release medium volume, C_i is the concentration of realgar at the ith time point, V_i is sampling volume, Q_n is cumulative release percentage at each time point, and C_0 is total drug concentration.

EGCG-RNPs (10.00 mg) were dissolved in 1 mL methanol, the unencapsulated nano-realgar was separated by ultrasound for 20 min and super centrifuge at 12,000 rpm, and the concentration of supernatant was determined by ICP-MS. The encapsulation efficiency (EE%) and drug loading (DL%) of EGCG-RNPs were determined by the following equations:

$$EE\% = W_E / W_A \times 100\% \tag{3}$$

$$DL\% = W_E / W_L \times 100\% \tag{4}$$

where W_E is the amount of entrapped nano-realgar in the EGCG-RNPs, W_A is the amount of nano-realgar added in the system, and W_L is the weight of EGCG-RNPs added in system.

Cell viability and proliferation

In vitro cytotoxicity of nanoparticles against APL HL-60 cells was evaluated using the MTT assay in the following three experimental groups: EGCG-RNPs, EGCG + RNPs, and Nano-realgar group (Zhang et al., 2014; Zhan et al., 2015). Cytotoxicity was evaluated across the range of 0.625, 1.25, 2.5, 5, 10, and 20 $\mu g \cdot mL^{-1}$ in triplicate for each group (Zhan et al., 2015). Absorbance was measured at 490 nm using a microplate reader (US Bio-Tek, model ELX800MV).

HL-60 cell uptake and efflux assay

Antiproliferative activity and uptake of RNPs into HL-60 cells were evaluated to determine whether the antiproliferative effect of nano-realgar on HL-60 cells was related to release characteristics of realgar from EGCG-RNPs (Orosz et al., 2017).

Eighty percent of the IC_{50} was used as the highest dose for the uptake and efflux experiment. Nano-realgar, EGCG + RNPs, and EGCG-RNPs were dissolved in DMSO at 1.25, 0.625, 0.313 $\mu g \cdot mL^{-1}$. The control group was treated with IMDM only. In the efflux group, cells were preincubated with the concentrations listed above for 6 h, resulting in uptake saturation. Cells were collected at 2, 5, 10, 20, 40, 60, 120, 180, and 240 min gather a group of cells ($n = 6$ at each time point). The As element concentration, which is representative of realgar was measured by ICP-MS (Hermo Electron ELEMENT 2, Thermo Electron Corporation, USA). Distribution profiles and IC_{50} of uptake and efflux were determined using GraphPad Prism® 7, and evaluate inhibition of uptake. The DAS 2.0 software fitted efflux $T_{1/2}$ and efflux rate (K_{out}).

Tumor model and experiment protocol

For a cancer treatment to be curative, the delivery system must competently localize to the tumor tissue and allow for internalization of the drug to reach all viable cells. After observing a robust anti-leukemic effect in vitro, we evaluated the anti-tumor effects of EGCG-RNPs in vivo. HL-60 cells were xenografted into NOD/SCID mice subcutaneously to establish a solid tumor model (Thompson et al., 2001; Stearns et al., 2010). The effects of intratumoral injections of EGCG-RNPs were evaluated.

HL-60 cells were cultured at 37 °C in an incubator with an atmosphere of 5% CO_2. Cells were collected in the logarithmic growth stage, then subcutaneously injected as a suspension into the backs of five NOD/SCID mice. Each mouse was inoculated with 5×10^6 cells in 100 μL. When the tumor volumes reached 300–500 mm^3, the tumor were excised and cut into 1 mm × 1 mm × 1 mm blocks. The cut tumor tissues were then implanted subcutaneously into the backs of 45 NOD/SCID mice. Antitumor experiments were performed when the mean tumor volume reached 140 mm^3 (Zhong et al., 2001).

Three NOD/SCID solid tumor model mice were selected as the blank group (G1, $n = 3$, physiological saline 20 μL). The other mice were divided into the following five groups: DOX

positive group (G2, $n = 6$, 11.25 mg $\cdot$ kg^{-1}), Nano-realgar group (G3, $n = 6$, 70 mg $\cdot$ kg^{-1}), high EGCG-RNPs (G4, $n = 10$, 70 mg $\cdot$ kg^{-1}), middle EGCG-RNPs (G5, $n = 10$, 35 mg $\cdot$ kg^{-1}), and low EGCG-RNPs (G6, $n = 10$, 17.5 mg $\cdot$ kg^{-1}). All groups were treated once per day for 13 consecutive days. The animals were weighed daily and their eating habits, mental status, and somatotype changes were observed at each weighing. Tumor volumes and weights were recorded every 3 days to allow for generation of body weight and tumor weight curves.

Tumor dimensions were measured using a linear caliper every 3 days until sacrifice and tumor volume (TV) was calculated using Equation (5). The relative tumor proliferation rate (T/C) was used as the indicator of antitumor activity of the treatments. T/C was calculated according to Equation (6), (T_{RTV}: RTV of treated group; C_{RTV}: RTV of control group), where RTV (relative tumor volume) $= V_t/V_0$, (V_t, tumor volume measured at the end of treatment; V_0, tumor volume measured at the beginning of treatment). The tumor growth inhibition rate (TGI) was calculated according to Equation (7), (C, average tumor volume/weight of the control group; T, average tumor volume/weight of the tested group). A curative effect was indicated by TGI $\geq$ 40% with $p < 0.05$.

$$V = (L \times S^2)/2 \tag{5}$$
$$T/C = (T_{RTV}/C_{RTV}) \times 100\% \tag{6}$$
$$\mathrm{TGI} = ((C-T))/C \tag{7}$$

Statistical analysis

All results are expressed as mean values ± standard deviation (SD). Data were evaluated using Student's t-test for comparisons between groups using Statistical Package for the Social Sciences ver. 13 software (SPSS, Chicago, IL). p values $<.05$ were considered to be significant.

Results and discussion

Transmission electron microscopy (TEM)

The morphological structure of EGCG-RNPs particles was characterized using TEM to confirm the formation of nano-realgar encapsulated in EGCG (Ye et al., 2014). The result showed that nano-realgar was an irregular rhomboid with uniform dispersion (Figure 1(A)). EGCG-RNPs prepared by chemical precipitation were irregular circles with a nearly uniform size distribution, uniform dispersion and no adhesion. Furthermore, EGCG-RNPs were irregular crystals that did not aggregated, resulting in a relatively narrow size distribution (Figure 1(B)). No obvious particle aggregation was observed.

Particle size and zeta potential

The average particle size of EGCG-RNPs was 200.3 ± 1.23 nm and the PDI was 0.071, indicating that the particles were within appropriate ranges suitable for intratumoral injection (Figure 2(A)). In general, particle aggregation is less likely to occur for charged particles with an optimum zeta potential due to electrostatic repulsion. The zeta potential of EGCG-RNPs was −46.8 ± 1.31 mV, particles are difficult to subside, condensation or aggregation, and has better stability (Zhang et al., 2014) (Figure 2(B)).

FTIR characterization of EGCG-RNPs

EGCG-RNPs were characterized by FTIR and compared with nano-realgar, EGCG, and EGCG + RNPs (Figure 2(C)). No peaks were present in nano-realgar spectra. EGCG showed characteristic peaks at 3372.23 cm^{-1} phenol group, 1695.73 cm^{-1} (stretching; for C $=$ O group), and 1458.49 cm^{-1} (stretching; for aromatic ring), EGCG + RNPs spectra showed a decrease in peaks associated with EGCG. However, in EGCG-RNPs, the strong peak at about 3371.45 cm^{-1}, which represented the phenol group of EGCG, disappeared, suggesting that phenolic hydroxyl groups associated with nano-realgar in EGCG-RNPs, further supporting successful EGCG-RNPs synthesis.

XRD characterization of EGCG-RNPs

XRD diffraction was evaluated for EGCG-RNPs, nano-realgar and EGCG (Figure 2(D)). The XRD pattern of nano-realgar contained strong diffraction peaks at 27.43° and 31.75°. The X-ray diffractogram of EGCG contained diffraction peaks at 16.15°, 21.73°, and 22.29°, and small sharp peaks at 28° to 40°. Characteristic peaks associated with EGCG and nano-realgar
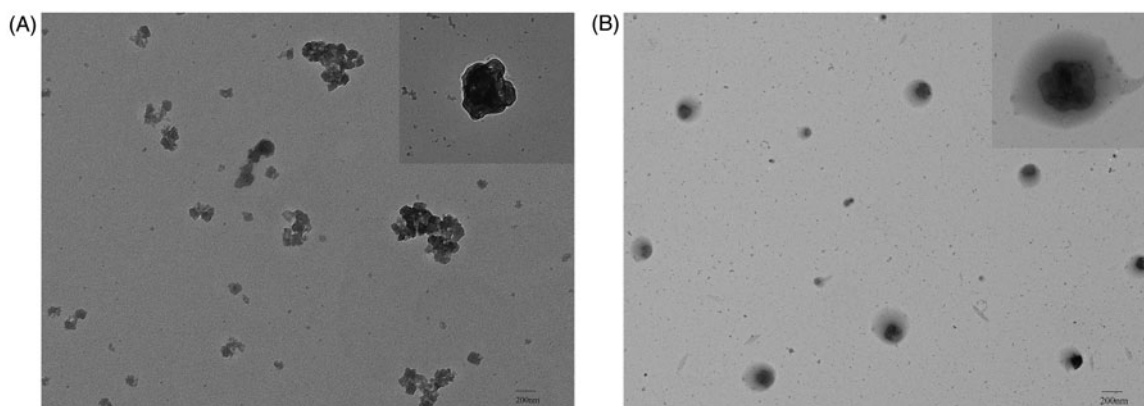

Figure 1. TEM images of nano-realgar (A, 200 nm, mag: ×1.2k, HV: 80.00 KV) and EGCG-RNPs (B, 200 nm, mag: ×1.2k, HV: 80.00KV).
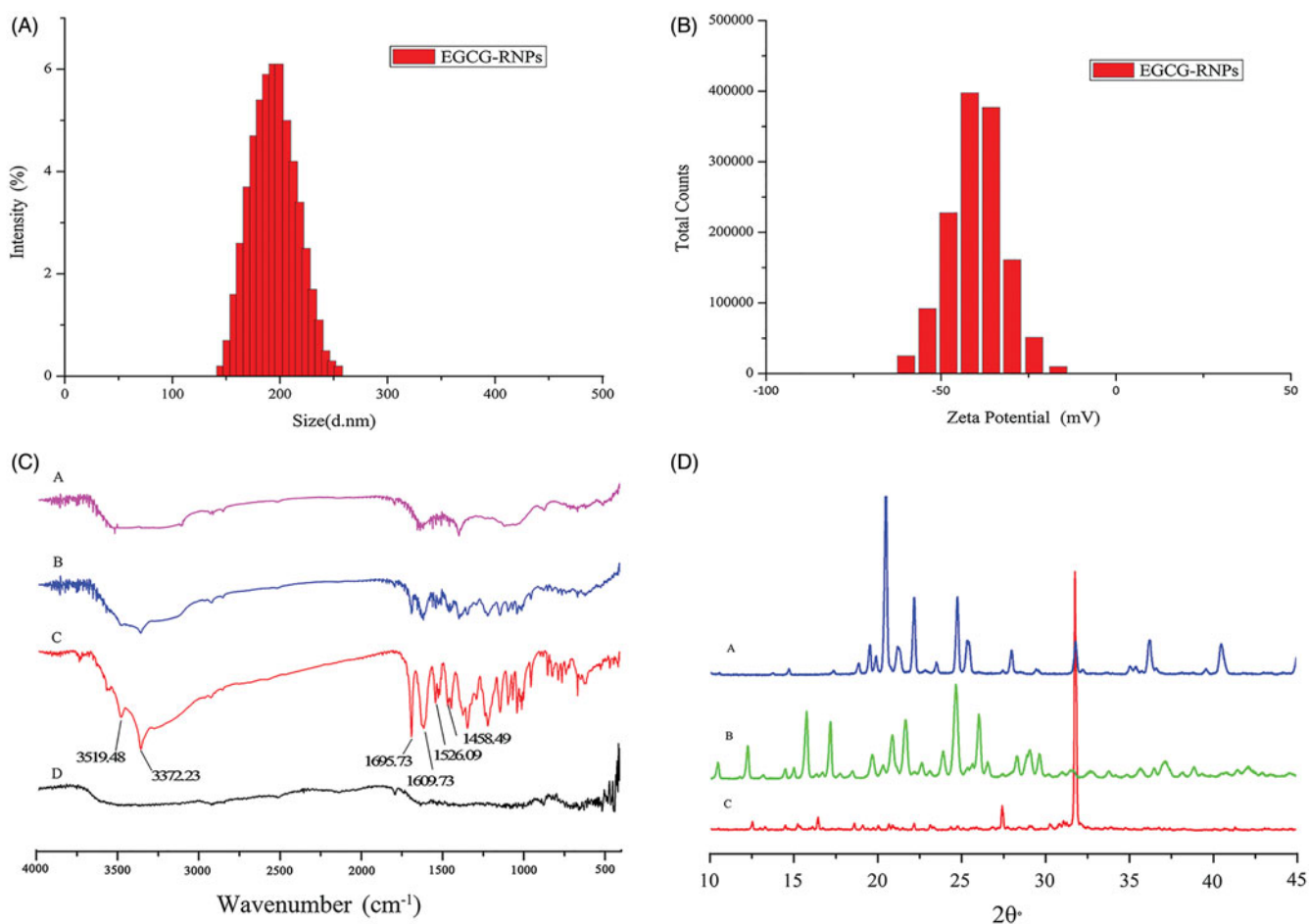
Figure 2. (A) The average particle size of EGCG-RNPs was 200.3 ± 1.23 nm and the PDI was 0.071. (B) The zeta potential was -46.8 ± 1.31 mV. (C) FTIR spectra of EGCG-RNPs, EGCG + RNPs, EGCG and nano-realgar. (D) XRD characterization of EGCG-RNPs, EGCG and nano-realgar.

were present at similar locations and intensities in EGCG-RNPs diffractograms, except that most of the sharp peaks had disappeared. XRD analysis confirmed that nano-realgar was nearly completely encapsulated in EGCG. However, chemical precipitation did not change the crystallinity of the realgar powder.

Characterization of EGCG-RNPs by DSC

An endothermic peak for EGCG was observed at 227.13 °C ($\triangle H$: 50.40 J·g^{-1}), demonstrating that EGCG was crystalline and in the anhydrous state. Nano-realgar had an endothermic peak at about 98.53 °C ($\triangle H$: 4.08 J·g^{-1}), which is the melting peak of nano-realgar. The DSC thermogram of EGCG + RNPs contained an endothermic peak at 234.8 °C ($\triangle H$: 3.37 J·g^{-1}). Comparison between EGCG and EGCG + RNPs showed reduced intensity and a slightly shifted in melting point, and the heat of transition was considerably reduced, which may have been due to structural changes in EGCG. The DSC thermogram of EGCG-RNPs contained an endothermic peak at 97.15 °C ($\triangle H$: 4.11 J·g^{-1}). The peak intensity of EGCG was disappeared which may be due to solubilization compared with EGCG-RNPs. The results indicated changes in crystallinity, and that the drug was uniformly dispersed in the EGCG-RNPs in the amorphous state,
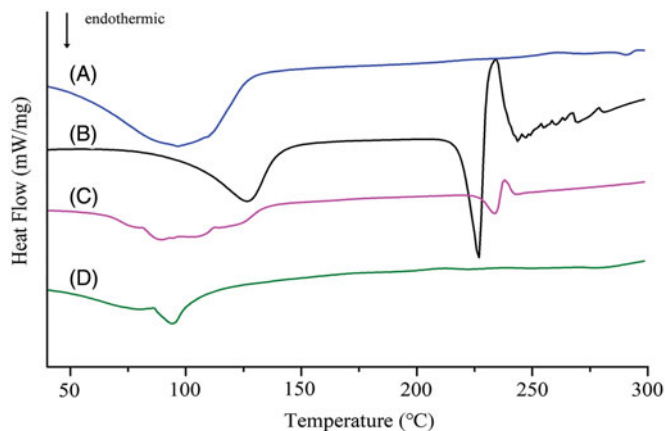

Figure 3. DSC of Nano-realgar (A), EGCG (B), EGCG + RNPs (C) and EGCG-RNPs (D).

with partial amorphization of both natural molecules in the nano-carrier system (Figure 3).

EGCG-RNPs release studies

The release profiles of realgar from EGCG-RNPs nanoparticles in PBS solution (pH 7.4) media at 37 °C are shown in Figure 4. The Q_n of nano-realgar was 74.61% at 7 h, 74.86% at 12 h,

respectively. Indicating the release rate and trend of nano-realgar does not have the characteristics of sustained and eased release. However, the Q_n for EGCG-RNPs was 45.91% at 7 h, 79.61% at 48 h, 79.85% at 72 h, respectively. The release rate and trend of EGCG-RNPs begin to ease after 7 h, showing the profiles of slow release (Supporting Information Material 1). Curve fitting showed that the release characteristics of nano-realgar conformed to the Higuchi equation model in vitro, and the drug release behavior of EGCG-RNPs conformed to the Weibull model with highest regression. This is unsurprising as it is considered as the most suitable kinetic model for drug release from polymeric matrices. The slow diffusion mechanism suggested can be due to the resistance to diffusive release of the conjugate by virtue of covalent attachment to EGCG (Zhang et al., 2014).
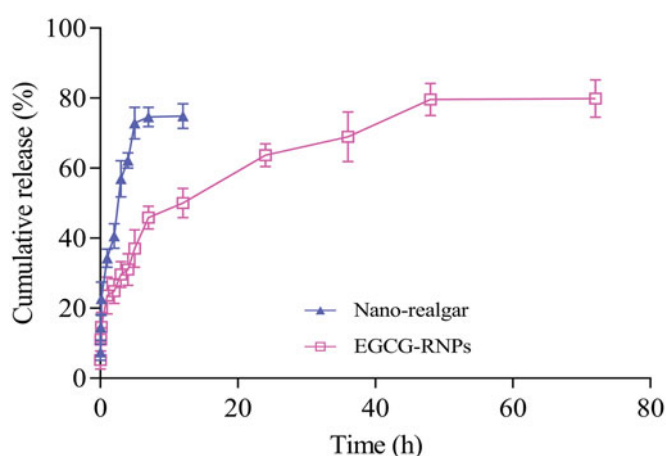

Figure 4. Release profiles of nano-realgar and EGCG-RNPs ($n = 3$, Mean ± SD).

Also, EGCG itself has a slow release characteristic. This will also contribute to the excellent sustained release properties. As a drug-loading material, EGCG-RNPs not only have the size effect and strong adsorption capacity of magnetic nano-particles, but also have a hydrophobic and hydrophilic cavity inside the cyclodextrin. The nano-realgar content in the EGCG-RNPs was measured using ICP-MS. The EE% and DL% of the nano-realgar in the EGCG-RNPs were 85.53% ± 3.26% and 5.63% ± 0.04%, respectively.

HL-60 cell inhibition in vitro

EGCG-RNPs, Nano-realgar, and EGCG + RNPs inhibited HL-60 cell growth in a concentration-dependent manner (Figure 5, Supporting Information Material 2). EGCG-RNPs inhibited HL-60 cell growth at the lowest concentrations. Nano-realgar and EGCG + RNPs did not differ in terms of inhibition rate of HL-60 cells. The IC_{50} values of EGCG-RNPs, Nano-realgar, and EGCG + RNPs were 1.384, 2.845, 2.891 $\mu g \cdot mL^{-1}$ as determined using Origin 8.5. The lower IC_{50} value of EGCG-RNPs indicated that this formulation was more potent than Nano-realgar or EGCG + RNPs. Both EGCG and Nano-realgar can inhibit cell growth and induce cell apoptosis in previous reports (Sylwia et al., 2003; Ning et al., 2005), respectively. We speculate that EGCG-RNPs also have the effect of induce cell apoptosis, which needs to be further verified by later experiments.

Uptake and efflux of EGCG-RNPs

The drug concentration according to IC_{50} value of EGCG-RNPs in the uptake and efflux experiments. The high, middle,
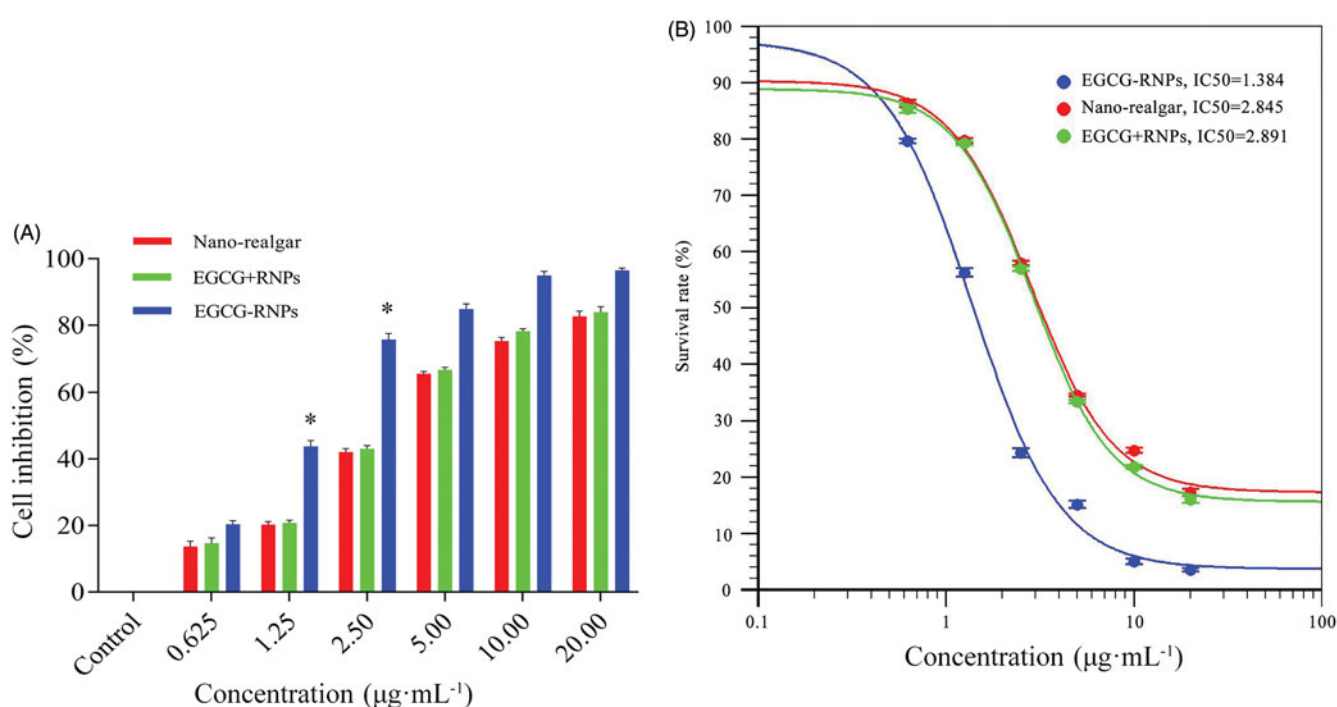

Figure 5. (A) Inhibitory effect of EGCG-RNPs on HL-60 cells ($n = 6$, Mean ± SD) and IC_{50} curve. At 1.25 $\mu g \cdot mL^{-1}$, 2.50 $\mu g \cdot mL^{-1}$, the inhibitory rate of EGCG-RNPs was significantly different than that of nano-realgar and EGCG + RNPs, *$p < 0.05$. (B) The IC_{50} values of Nano-realgar, EGCG + RNPs, and EGCG-RNPs on HL-60 cells were 2.854, 2.891, and 1.384 $\mu g \cdot mL^{-1}$, respectively. Blue represents EGCG-RNPs, green represents EGCG + RNPs, and red represents nano-realgar.
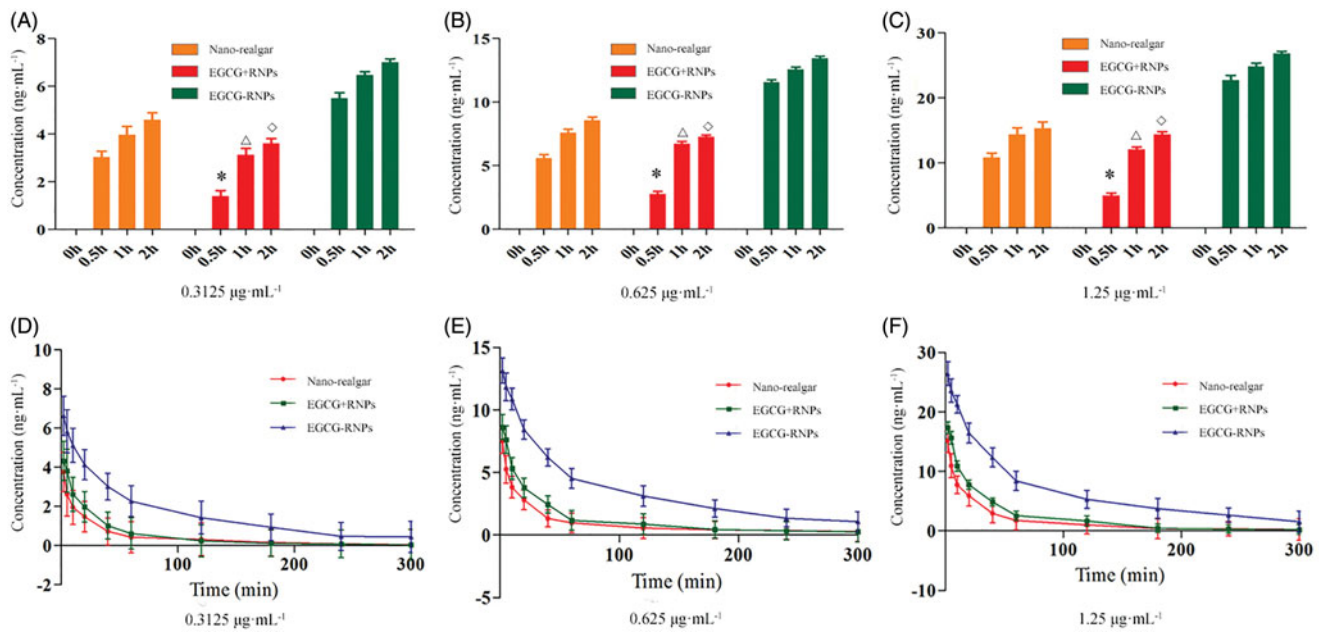
Figure 6. The impact of EGCG-RNPs on HL-60 cell uptake and efflux ($n = 6$, Mean ± S). (A, D): 0.3125 $\mu g \cdot mL^{-1}$, (B, E): 0.625 $\mu g \cdot mL^{-1}$, (C, F): 1.25 $\mu g \cdot mL^{-1}$. Cells were treated with 0.3125, 0.625, 1.25 $\mu g \cdot mL^{-1}$ of nano-realgar, EGCG + RNPs, or EGCG-RNPs for 0, 0.5, 1, and 2 h, and intracellular nano-realgar concentration was measured(A, B, C). Cells were treated with 0.3125, 0.625, or 1.25 $\mu g \cdot mL^{-1}$ of nano-realgar, EGCG + RNPs, or EGCG-RNPs for 6 h, and intracellular nano-realgar concentration was measured (D, E, F). Data shown are means ± standard deviations for six samples. *Significantly different from the EGCG-RNPs group at 0.5 h, $p < 0.05$. △Significantly different from the EGCG-RNPs group at 1 h, $p < 0.05$. ◇Significantly different from the EGCG-RNPs group at 2 h, $p < 0.05$.

and low concentrations were 1.25, 0.625, and 0.3125 $\mu g \cdot mL^{-1}$. The results are shown in Figure 6. In the EGCG + RNPs groups, the uptake of As was lower than that in the Nano-realgar group, at 120 min in the high dose condition, the amount of As in the cells in the EGCG + RNPs group was nearly equal to that in the Nano-realgar group, after which the concentration of As did not increase. In the EGCG-RNPs group, As uptake by HL-60 cells occurred in a dose-dependent manner, and was higher than the other groups.

Uptake results showed that the concentration of As in cells did not increase after 120 min, suggesting that uptake was saturated. Therefore, the drug incubation time was set at 2 h to saturate uptake for efflux experiments. The high, middle, and low concentrations were 1.25, 0.625, and 0.3125 $\mu g \cdot mL^{-1}$. The cells were evaluated at different time points and As in cells was determined by ICP-MS. As shown in Figure 6(D–F), intracellular As concentration was highest in the EGCG-RNPs group, indicating that the cells exhibited slower efflux of As in this group. As shown in Table 1, the $T_{1/2}$ was 29.275 min and the efflux rate (K_{out}) was 0.024 $ng \cdot min^{-1}$, which was significantly different from those in the Nano-realgar and EGCG + RNPs treated cells ($p < 0.05$), which might be due to prolonged retention of As in the cells by EGCG.

On the basis of these results, we hypothesized that EGCG-RNPs may bind to a specific receptor or transporter on the cell surface, or these functionalized EGCG-RNPs could increase the hydrophobicity of cell suspension, greatly decrease the peak potential of cell, and facilitate the cellular uptake of the Nano-realgar into HL-60 leukemia cells. Previous studies have reported that the P-glycoprotein pump (P-gp) is an important efflux pump for a variety of anticancer

Table 1. Results of the $T_{1/2}$ and K_{out} ($n = 6$, ± S).

Groups (0.625 $\mu g \cdot mL^{-1}$)	$T_{1/2}$ (min)	K_{out} (min^{-1})
Nano-realgar	7.828 ± 1.05*	0.089 ± 0.024*
EGCG + RNPs	11.192 ± 1.86*	0.062 ± 0.018*
EGCG-RNPs	29.275 ± 2.58	0.024 ± 0.008

Significantly different from the EGCG-RNPs group at *$p < 0.05$.

drugs such as alkaloids, anthracyclines, and paclitaxel (Yong et al., 2015). EGCG can regulate P-gp function. After EGCG-RNPs enter cells, nano-realgar is released from EGCG, and EGCG inhibit the function of P-gp to improve the relevant drug accumulation in drug-resistant cancer cells and enhance the cytotoxicity suppression of nano-realgar, demonstrated by the finding that the concentration of intracellular nano-realgar remains high. This set of experiments showed that the combination of EGCG and nano-realgar has a significant effect on increasing drug uptake and prolonged drug efflux.

In vivo inhibiton effect of HL-60 cell solid tumor

High (G4), medium (G5), and low (G6) doses of EGCG-RNPs inhibited tumor growth after 13 days of treatment by 60.18, 50.82, and 31.41% ($p < .05$), respectively, indicating dose-dependent inhibition. The intergroup p values were 0.01126, 0.12491, and 0.22072, indicating that only the G4 group was significantly different. The mean tumor volumes reduction in the DOX group (G2), the Nano-realgar group, and the EGCG-RNPs group were greater than those in the blank control group (G1) (Figure 7(A,B)). We found that high (G4), medium (G5), and low (G6) doses of EGCG-RNPs decreased tumor weight by 75.82, 41.77, and 40.30% ($p < 0.05$), respectively, compared with the tumor weights on day 1 (Figure 7(C)). The weight loss ratios of EGCG-RNPs mice in response to

high (G4), medium (G5), and low (G6) doses were −1.15, 0.82, and −3.02% ($p < 0.05$), respectively (Figure 7(D); Supporting Information Material 3).

EGCG-RNPs had an obvious inhibitory effect on tumor growth, which was close in magnitude to that of the antitumor drug DOX. The growth inhibition rate in the high dose group (G4) was significantly higher than that in the low dose group (G6), indicating that EGCG-RNPs exerted inhibitory effects in a dose-dependent manner. However, there were no significant changes in body weight of the mice,
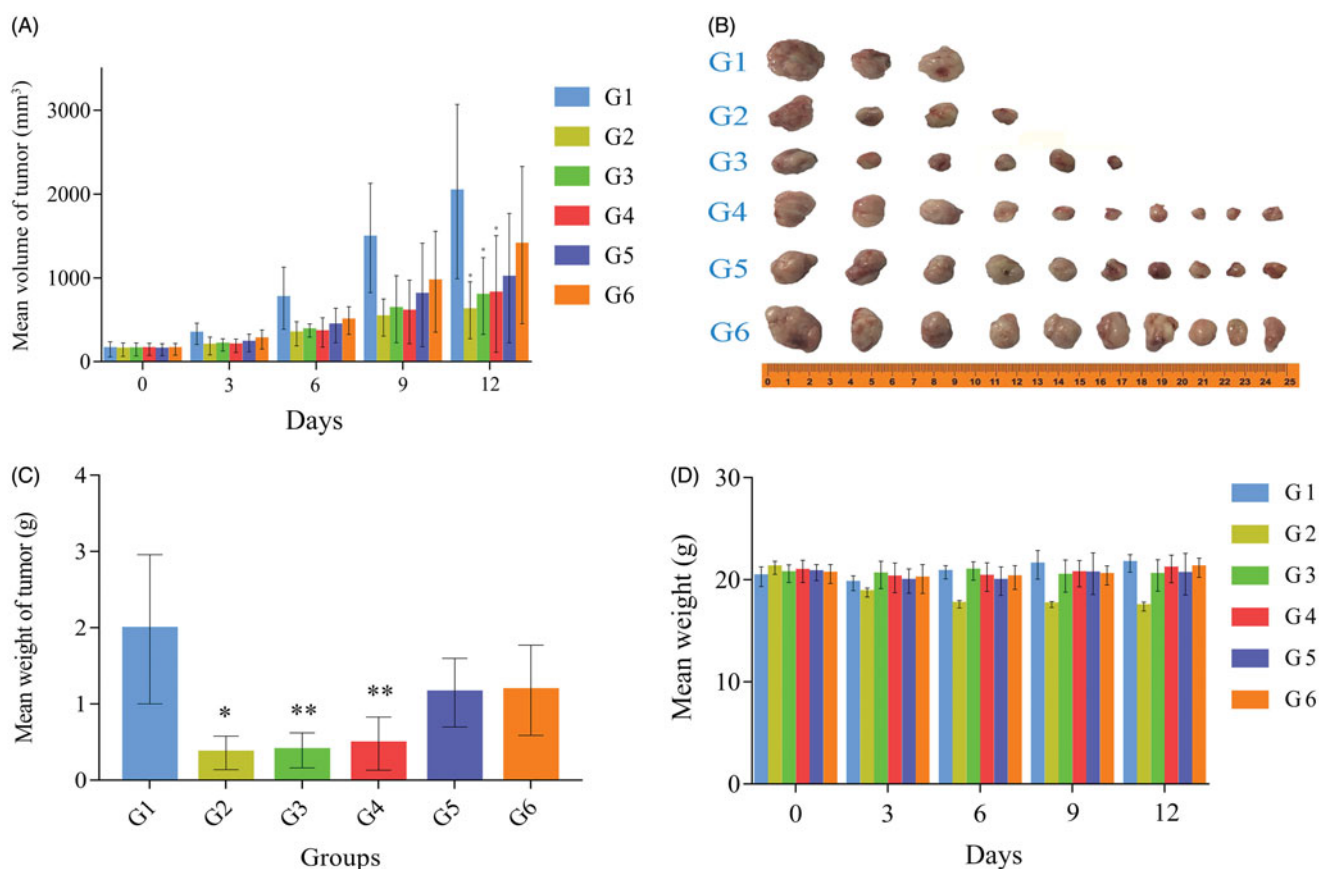

Figure 7. Tumor volume growth curve (A), solid tumor sample (B) (two mice died during the experiment), mean tumor weight (C), weight change of NOD.SCID mice (D). The blank group (G1, three, physiological saline 20 μL), DOX positive group (G2, six, 11.25 mg·kg^{-1}), nano-realgar group (G3, six, 70 mg·kg^{-1}), and high (G4, ten, 70 mg·kg^{-1}), middle (G5, ten, 35 mg·kg^{-1}), and low (G6, ten, 17.5 mg·kg^{-1}) EGCG-RNPs groups. All groups were treated once per day for 13 consecutive days. *, **Significantly different from the G1 group, $p < 0.05$ and $p < 0.01$, respectively.
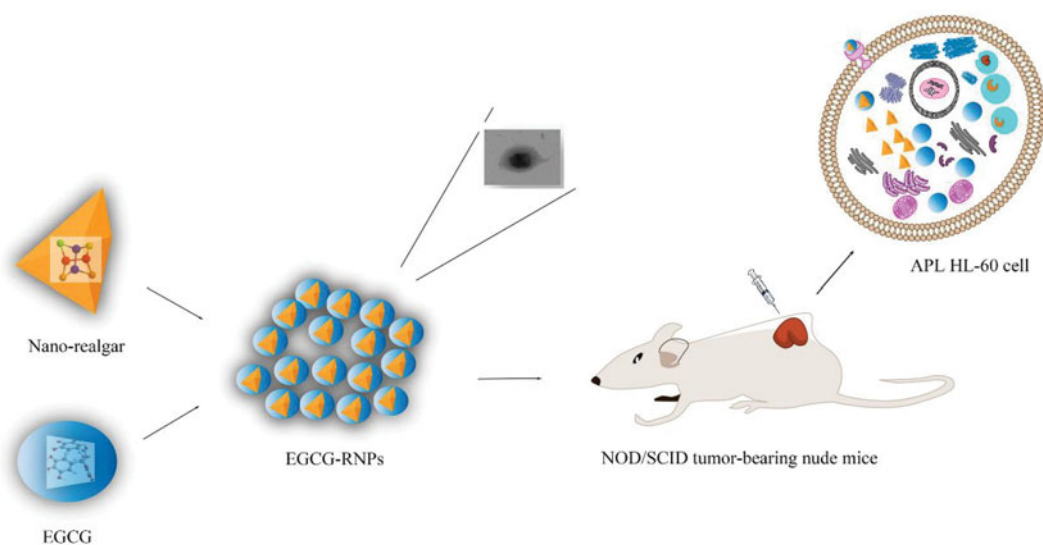
Scheme 1. In this work, the objective was to develop a new class of nanoparticles, EGCG-RNPs (nano-realgar encapsulated in EGCG), which can enhance anti-proliferative effect of APL HL-60 leukemia cells by increased uptake and prolonged the retention time of realgar, and therapeutic effect on subcutaneous HL-60 cells solid tumor.

indicating that EGCG-RNPs did not affect eating or drinking behaviors of tumor-bearing mice during treatment (Ting et al., 2010).

Conclusions

In this study, we successfully developed a new method for producing EGCG-encapsulated nano-realgar nanoparticles (EGCG-RNPs) by chemical coprecipitation. EGCG-RNPs significantly inhibited the growth of APL HL-60 cells. The average particle sizes were suitable for intratumoral injection and properties of EGCG were different in this formulation, as demonstrated by disappearance of hydroxyl peaks in FTIR spectra, and conversion to the amorphous form. EGCG-RNPs significantly inhibited APL HL-60 cell proliferation activity and retention in HL-60 cells was greatly increased *in vitro*. Furthermore, EGCG-RNPs exerted an obvious inhibitory effect on tumor growth. However, the specific mechanisms of HL-60 cell uptake and efflux of EGCG-RNPs require further study. Consequently, these nanoparticles have excellent potential for use as anti-tumor treatments, and may be suitable for use in human cancer therapy studies and clinical trials.

Ethical approval

All animal experiments were approved by the Animal Management and Ethics Committee of Anhui University of Chinese Medicine.

Disclosure statement

No potential conflict of interest was reported by the authors.

References

Acevedo KM, Hayne DJ, Mcinnes LE, et al. (2018). The effect of structural modifications to glyoxalbis(thiosemicarbazonato) copper(II) complexes on cellular copper uptake, copper-mediated ATP7A trafficking and *P*-glycoprotein mediated efflux. J Med Chem 61:711–23.

Baláž P, Fabián M, Pastorek M, et al. (2009). Mechanochemical preparation and anticancer effect of realgar As$_4$S$_4$ nanoparticles. Mater Lett 63:1542–4.

Bing H, Yuwen T, Xiaoxiong Z, et al. (2013). Bioactive peptides/chitosan nanoparticles enhance cellular antioxidant activity of (-)-epigallocatechin-3-gallate. J Agric Food Chem 61:875–81.

Chih-Yeu F, Chung-Chun W, Hui-Yu H, et al. (2015). EGCG inhibits proliferation, invasiveness and tumor growth by up-regulation of adhesion molecules, suppression of gelatinases activity, and induction of apoptosis in nasopharyngeal carcinoma cells. Int J Mol Sci 16:2530–58.

Dongxu W, Yijun W, Xiaochun W, et al. (2015). Green tea polyphenol (-)-epigallocatechin-3-gallate triggered hepatotoxicity in mice: responses of major antioxidant enzymes and the Nrf2 rescue pathway. Toxicol Appl Pharmacol 283:65–74.

Farabegoli F, Papi A, Bartolini G, et al. (2010). (-)-Epigallocatechin-3-gallate downregulates Pg-P and BCRP in a tamoxifen resistant MCF-7 cell line. Phytomedicine 17:356–62.

Hajipour H, Hamishehkar H, Nazari SAS, et al. (2018). Improved anticancer effects of epigallocatechin gallate using RGD-containing nanostructured lipid carriers. Artif Cells Nanomed Biotechnol 46:1–10.

Higdon JV, Balz F. (2003). Tea catechins and polyphenols: health effects, metabolism, and antioxidant functions. CRC Crit Rev Food Technol 43: 89–143.

Hsieh DS, Lu HC, Chen CC, et al. (2012). The preparation and characterization of gold-conjugated polyphenol nanoparticles as a novel delivery system. Int J Nanomed 7:1623–33.

Jie ZZ, Zhou Q, Zhi WJ, et al. (2011). Validation of the crystal structure of medicinal realgar in China. Spectrosc Spectr Anal 31:291–6.

Kazushige K. (2005). Comment on inhibitory effect of (-)-epigallocatechin 3-gallate, a polyphenol of green tea, on neutrophil chemotaxis in vitro and in vivo. J Agric Food Chem 53:1307–8.

Mauro F. (2005). Cancer nanotechnology: opportunities and challenges. Nat Rev Cancer 5:161–71.

Mcculloch D, Brown C, Iland H. (2017). Retinoic acid and arsenic trioxide in the treatment of acute promyelocytic leukemia: current perspectives. Oncotargets Ther Ott 10:1585–601.

Moradzadeh M, Roustazadeh A, Tabarraei A, et al. (2017). Epigallocatechin-3-gallate enhances differentiation of acute promyelocytic leukemia cells via inhibition of PML-RARα and HDAC1. Phytother Res Ptr 32.

Ning N, Peng ZF, Yuan L, et al. (2005). Realgar nano-particles induce apoptosis and necrosis in leukemia cell lines K562 and HL-60. China J China Mater Med 30:136–40.

Orosz Á, Bősze S, Mező G, et al. (2017). Oligo- and polypeptide conjugates of cationic porphyrins: binding, cellular uptake, and cellular localization. Amino Acids 49:1263–14.

Philipp S, Marie-Thérèse S, Heike S, et al. (2015). Epigallocatechin gallate, ellagic acid, and rosmarinic acid perturb dNTP pools and inhibit de novo DNA synthesis and proliferation of human HL-60 promyelocytic leukemia cells: synergism with arabinofuranosylcytosine. Phytomedicine 22:213–22.

Ravi S, Nripen C, Ajit Z, et al. (2012). Laminin receptor specific therapeutic gold nanoparticles (198AuNP-EGCg) show efficacy in treating prostate cancer. Proc Natl Acad Sci USA 109:12426–31.

Ryan P, Hynes MJ. (2007). The kinetics and mechanisms of the complex formation and antioxidant behaviour of the polyphenols EGCg and ECG with iron(III). J Inorg Biochem 101:585–93.

Shanshan W, Kang S, Xin W, et al. (2013). Protonation of epigallocatechin-3-gallate (EGCG) results in massive aggregation and reduced oral bioavailability of EGCG-dispersed selenium nanoparticles. J Agric Food Chem 61:7268–75.

Shen Y, Shen ZX, Yan H, et al. (2001). Studies on the clinical efficacy and pharmacokinetics of low-dose arsenic trioxide in the treatment of relapsed acute promyelocytic leukemia: a comparison with conventional dosage. Leukemia 15:735–41.

Stearns ME, Amatangelo MD, Varma D, et al. (2010). Combination therapy with epigallocatechin-3-gallate and doxorubicin in human prostate tumor modeling studies: inhibition of metastatic tumor growth in severe combined immunodeficiency mice. Am J Pathol 177: 3169–79.

Sun LM, Zhang CL, Ping L. (2011). Characterization, antimicrobial activity, and mechanism of a high-performance (∼)-epigallocatechin-3-gallate (EGCG)-Cu∼(II)/polyvinyl alcohol (PVA) nanofibrous membrane. J Agric Food Chem 59:5087–92.

Sylwia B, Elzbieta G, Teresa W, et al. (2003). Induction of apoptosis by EGCG in selected tumour cell lines in vitro. Folia Histochem Cytobiol 41:229.

Tallman MS, Chadi N, Feusner JH, et al. (2002). Acute promyelocytic leukemia: evolving therapeutic strategies. Blood 99:759.

Tanaka Y, Komatsu H, Ishii K, et al. (2000). Successful treatment of relapsed and refractory acute promyelocytic leukemia with arsenic trioxide (As_2O_3). [Rinsho ketsueki] Jpn J Clin Hematol 41:354.

Thompson J, Guichard SM, Cheshire PJ, et al. (2001). Development, characterization and therapy of a disseminated model of childhood neuroblastoma in SCID mice. Cancer Chemother Pharmacol 47: 211–21.

Ting L, Jiao W, Yancun Y, et al. (2010). (-)-Epigallocatechin gallate sensitizes breast cancer cells to paclitaxel in a murine model of breast carcinoma. Breast Cancer Res 12:R8–R8.

Wang XB, Rong-Gang XI, Shi Y, et al. (2008). Preparation studies of realgar nano-particles. Pharma J Chin People's Liber Army. 6:12–18.

Yao S, Zhong L, Chen M, et al. (2017). Epigallocatechin-3-gallate promotes all-trans retinoic acid-induced maturation of acute promyelocytic leukemia cells via PTEN. Int J Oncol 51:899–906.

Ye T, Wang X, Xi R, et al. (2014). Enhanced antitumor activity of realgar mediated by milling it to nanosize. Int J Nanomed 9:745–57.

Yong Z, Shao-Xiang W, Ji-Wei M, et al. (2015). EGCG inhibits properties of glioma stem-like cells and synergizes with temozolomide through downregulation of P-glycoprotein inhibition. J Neurooncol 121:41–52.

Zhan XQ, Zhao FM, Biology DO. (2015). Realgar nanoparticles inhibiting the proliferation of tumor cells in vitro and in vivo. Chin J Cancer Prevent Treat 22:184–8.

Zhong RK, Winkel JGVD, Thepen T, et al. (2001) Cytotoxicity of anti-CD64-ricin A chain immunotoxin against human acute myeloid leukemia cells in vitro and in SCID Mice. Journal of Hematotherapy & Stem Cell Research 10(1):95–105.

Zhang L, Wu S, Wang D, et al. (2014) Epigallocatechin-3-gallate (EGCG) in or on nanoparticles: enhanced stability and bioavailability of EGCG encapsulated in nanoparticles or targeted delivery of gold nanoparticles coated with EGCG. Handbook Nanotoxicol Nanomed Stem Cell Toxicol 134–144.

Zhou L, Chen M, Tian L, et al. (2013). Release of polyphenolic drugs from dynamically bonded layer-by-layer films. Acs Appl Mater Interfaces 5: 3541–8.